"Dressing" lines and vertices in calculations of matrix elements with the coupled-cluster method and determination of Cs atomic properties

Andrei Derevianko

Department of Physics, University of Nevada, Reno, Nevada 89557, USA

Sergey G. Porsev

Department of Physics, University of Nevada, Reno, Nevada 89557, USA
and Petersburg Nuclear Physics Institute, Gatchina, Leningrad district, 188300, Russia

We consider evaluation of matrix elements with the coupled-cluster method. Such calculations formally involve infinite number of terms and we devise a method of partial summation (dressing) of the resulting series. Our formalism is built upon an expansion of the product $C^\dagger C$ of cluster amplitudes C into a sum of n-body insertions. We consider two types of insertions: particle (hole) line insertion and two-particle (two-hole) random-phase-approximation-like insertion. We demonstrate how to "dress" these insertions and formulate iterative equations. We illustrate the dressing equations in the case when the cluster operator is truncated at single and double excitations. Using univalent systems as an example, we upgrade coupled-cluster diagrams for matrix elements with the dressed insertions and highlight a relation to pertinent fourth-order diagrams. We illustrate our formalism with relativistic calculations of the hyperfine constant $A(6s)$ and the $6s_{1/2}-6p_{1/2}$ electric-dipole transition amplitude for the Cs atom. Finally, we augment the truncated coupled-cluster calculations with otherwise omitted fourth order diagrams. The resulting analysis for Cs is complete through the fourth order of many-body perturbation theory and reveals an important role of triple and disconnected quadruple excitations.

I. INTRODUCTION

The coupled-cluster (CC) method [1,2] is a powerful and ubiquitous technique for solving quantum many-body problems. Let us briefly recapitulate general features of the CC method, so we can motivate our further discussion. At the heart of the CC method lies the exponential ansatz for the exact many-body wave function

$$|\Psi_i\rangle = \exp(T_i)|0_i\rangle = \left(1 + T_i + \frac{1}{2!}T_i^2 + \cdots\right)|0_i\rangle. \quad (1)$$

Here $T_i = \Sigma_k T_i^{(k)}$ is the cluster operator involving amplitudes $T_i^{(k)}$ of k-fold particle-hole excitations from the reference Slater determinant $|0_i\rangle$. The parametrization (1) is derived from rigorous resummation of many-body perturbation theory (MBPT) series. From solving the eigenvalue equation one determines the cluster amplitudes and the associated energies. While the ansatz (1) contains an *infinite* number of terms due to expansion of the exponent, the resulting equations for cluster amplitudes $T_i^{(k)}$ contain a *finite* number of terms. This simplifying property is unfortunately lost when the resulting wave functions are used in calculations of matrix elements: upon expansion of exponents the number of terms becomes infinite. Indeed, consider matrix elements of an operator Z, e.g., the transition amplitude between two states

$$\mathcal{M}_{ij} = \frac{Z_{ij}}{\sqrt{N_i N_j}}, \quad (2)$$

with normalization $N_i = \langle\Psi_i|\Psi_i\rangle$. It is clear that both the numerator and denominator have infinite numbers of terms, e.g.,

$$Z_{ij} = \langle\Psi_i|Z|\Psi_j\rangle = \sum_{\lambda=0}^{\infty}\sum_{\mu=0}^{\infty}\frac{1}{\lambda!\,\mu!}\langle 0_i|(T_i^\dagger)^\lambda Z(T_j)^\mu|0_j\rangle. \quad (3)$$

In this paper we address the question of partially summing the terms of the above expansion for matrix elements, so that the result subsumes an infinite number of terms.

More specifically we are interested in transitions between states of univalent atoms, such as alkali-metal atoms. There has been a number of relativistic coupled-cluster calculations for these systems [3–9]. In particular, calculations [3–6] ignore the nonlinear terms ($\lambda > 1$ and $\mu > 1$) in the expansion (3); we will designate this approximation as the linearized coupled-cluster (LCC) method. At the same time, it is well established that for univalent atoms an important chain of many-body diagrams for matrix elements comes from the so-called random-phase approximation (RPA). A direct comparison of the RPA series and the truncated LCC expansion in Ref. [10] leads to the conclusion that a fraction of the RPA chain is missed due to the omitted nonlinear terms. One of the methods to correct for the missing RPA diagrams has been investigated in Ref. [4]. These authors replaced the bare matrix elements with the dressed matrix elements as prescribed by the RPA method. Such a direct RPA dressing involved a partial subset of diagrams already included in the

CC method, i.e., it leads to a double counting of diagrams. To partially rectify this shortcoming, the authors of Ref. [4] have manually removed certain leading-order diagrams, higher-order terms being doubly counted. Here we present an alternative infinite-summation scheme for RPA chain that avoids the double counting and thus a manual removal of the "extra" diagrams.

In addition to the RPA-like dressing of the coupled-cluster diagrams for matrix elements, we consider another subset of diagrams that leads to a dressing of particle and hole lines in the CC diagrams. The leading-order corrections due to the dressing scheme presented here arise in the fourth order of MBPT, and in this paper we present a detailed comparison with the relevant fourth-order diagrams. Finally, we illustrate our approach with relativistic computation of hyperfine-structure constants and dipole matrix elements for the Cs atom. In addition to dressing corrections we incorporate certain classes of diagrams from the direct fourth-order MBPT calculation (as in Refs. [10,11]), so that the result is complete through the fourth order. To the best of our knowledge, the reported calculations are the first calculations for Cs complete through the fourth order of MBPT.

The paper is organized as follows. First, we present a more extensive discussion of the CC formalism in Sec. II. In Sec. III we partition a product of CC operators into a set of insertion operators. With these insertions, we dress particle and hole lines in Sec. IV, and discuss RPA-like dressing in Sec. V. The present paper may be considered as an all-order extension of the fourth-order calculation [10,11], and in Sec. VI we present an illustrative comparison with the fourth-order diagrams. Finally, the designed summation schemes are illustrated numerically in Sec. VII and the conclusions are drawn in Sec. VIII. Unless noted otherwise, atomic units $\hbar = |e| = m_e \equiv 1$ are used throughout the paper. We follow the convention of Ref. [12] for drawing Brueckner-Goldstone diagrams.

II. COUPLED-CLUSTER FORMALISM FOR UNIVALENT SYSTEMS

In this section we specialize our discussion of the coupled-cluster method to atomic systems with one valence electron outside the closed-shell core. We review various approximations and summarize the CC formalism for calculation of matrix elements.

We are interested in solving the atomic many-body problem. The total Hamiltonian H is partitioned as

$$H = H_0 + G, \qquad (4)$$

where H_0 is the suitably chosen lowest-order Hamiltonian and the residual interaction $G = H - H_0$ is treated as a perturbation. For systems with one valence electron outside the closed-shell core, a convenient choice for H_0 is the frozen-core (V^{N-1}) Hartree-Fock Hamiltonian [13]. In the following, we explicitly specify the state v of the valence electron, so that the proper reference eigenstate $|0_i\rangle$ of H_0 is $|0_v\rangle = a_v^\dagger|0_c\rangle$, where the pseudovacuum state $|0_c\rangle$ specifies the occupied core.

For open-shell systems a general CC parametrization reads [12]

$$|\Psi_i\rangle = \{\exp(T_i)\}|\Phi_i\rangle, \qquad (5)$$

where the curly brackets denote normal products of operators. For univalent systems the above ansatz may be simplified to

$$|\Psi_v\rangle = \exp(C) \, S_v a_v^\dagger|0_c\rangle = \left(\sum_{\mu=0}^\infty \frac{(C)^\mu}{\mu!}\right) S_v a_v^\dagger|0_c\rangle. \qquad (6)$$

Here C represents the cluster operator involving (single, double, triple, etc.) excitations of core orbitals

$$C = C^{(1)} + C^{(2)} + \cdots = \sum_{ma} \rho_{ma} a_m^\dagger a_a + \frac{1}{2!} \sum_{mnab} \rho_{mnab} a_m^\dagger a_n^\dagger a_b a_a$$

$$+ \cdots, \qquad (7)$$

and S_v incorporates additional excitations from the valence state v,

$$S_v = 1 + S_v^{(1)} + S_v^{(2)} + \cdots$$

$$= 1 + \sum_m \rho_{mv} a_m^\dagger a_v + \sum_{mna} \rho_{mnva} a_m^\dagger a_n^\dagger a_a a_v + \cdots. \qquad (8)$$

In these formulas and throughout the paper we employ the following labeling convention: indices a, b, c, d denote single-particle states occupied in the core $|0_c\rangle$ and indices m, n, r, s, t stand for the remaining (virtual) orbitals. In this convention the valence states v and w form a subset of the virtual orbitals. Finally, indices i, j, k, l stand for any of the above classes of single-electron orbitals. In Eqs. (7) and (8) the cluster amplitudes ρ_{ij} stand for single-particle excitations and ρ_{ijkl} for two-particle excitations, with an apparent generalization to k-fold excitation amplitudes.

Dictated by the computational complexity, in most applications the cluster operator is truncated at single and double excitations (CCSD approximation): $C \approx C^{(1)} + C^{(2)}$ and $S_v \approx 1 + S_v^{(1)} + S_v^{(2)}$. A further *linearized* (LCCSD) approximation consists in neglecting nonlinear terms in the expansion of the exponent in Eq. (5), i.e.,

$$|\Psi_v\rangle^{\text{LCCSD}} \equiv (1 + S_v^{(1)} + S_v^{(2)} + C^{(1)} + C^{(2)})|0_v\rangle. \qquad (9)$$

.

As discussed in the Introduction, the cluster amplitudes can be found from solving a proper analog of the eigenvalue equation. We assume that these equations are solved and in a typical application we are faced with the necessity of computing matrix elements, Eq. (2), between two many-body wave functions $|\Psi_v\rangle$ and $|\Psi_w\rangle$. As demonstrated by Blundell *et al.* [3], so-called disconnected diagrams [12] in the numerator and the denominator of Eq. (2) cancel. Their final expression for the exact matrix element reads

$$\mathcal{M}_{wv} = \delta_{wv}(Z^{\text{core}})_{\text{conn}} + \frac{(Z_{wv}^{\text{val}})_{\text{conn}}}{\{[1 + (N_v^{\text{val}})_{\text{conn}}][1 + (N_w^{\text{val}})_{\text{conn}}]\}^{1/2}}, \qquad (10)$$

where the matrix element Z_{wv}, Eq. (3), is split into core Z^{core} and valence Z_{wv}^{val} contributions, the diagrams comprising Z^{core} being independent of the valence indices. The valence and core parts of the normalization factor N_v are defined in a
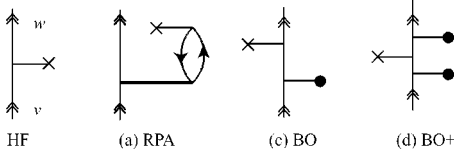
FIG. 1. Dominant LCCSD contributions for the matrix elements. The double arrows represent the valence state, crosses represent matrix elements z_{ij}, and heavy horizontal lines represent cluster amplitudes. In particular, the RPA diagram involves valence doubles and the BO diagram involves valence singles. Here and below we do not draw the exchange variants for the diagrams.

similar fashion. Notice that all the diagrams in Eq. (10) must be rigorously connected as emphasized by subscripts "conn." Since the total angular momentum of the closed-shell core is zero, the core contribution Z^{core} vanishes for nonscalar (and pseudoscalar) operators and in the following discussion we will mainly focus on Z^{val}_{wv}.

Blundell *et al.* [3] have employed the LCCSD parametrization for the wave function (9) to derive 21 diagrams for Z^{val}_{wv} and five contributions to N^{val}_v. The LCCSD contributions to Z^{core} can be found in Ref. [14]. It is the goal of this paper to go beyond these linearized LCCSD contributions. The LCCSD approximation will provide us with "skeleton" diagrams that will be "dressed" due to nonlinear CC terms. We display representative LCCSD diagrams in Fig. 1. In a typical calculation, the dominant correction to the Hartree-Fock (HF) value arise from RPA-type diagram (a) and Brueckner-orbital (BO) diagrams (c) and (d). (We retain the original enumeration scheme of Ref. [3] for the diagrams.) Here are the corresponding algebraic expressions for these LCCSD contributions:

$$Z^{(\text{HF})}_{wv} = z_{wv},$$

$$Z^{(\text{a})}_{wv} = \sum_{ma} z_{am}\tilde{\rho}_{wmva} + \text{H.c.s.},$$

$$Z^{(\text{c})}_{wv} = \sum_{m} z_{wm}\rho_{mv} + \text{H.c.s},$$

$$Z^{(\text{d})}_{wv} = \sum_{mn} z_{mn}\rho^*_{mw}\rho_{nv}, \qquad (11)$$

where H.c.s. denotes Hermitian conjugation of the preceding term with a simultaneous swap of the valence indices $w \leftrightarrow v$. Throughout the paper we use the following definition of quantities with tildes, $\tilde{A}_{ijkl} = A_{ijkl} - A_{jikl}$. In particular, in the above equations, $\tilde{\rho}_{wmva} = \rho_{wmva} - \rho_{mwva}$.

III. GENERATING OBJECT $C^{\dagger}C$

At this point we have reviewed application of the coupled-cluster method to computing properties of univalent systems. In the remainder of this paper we deal with the mathematical object
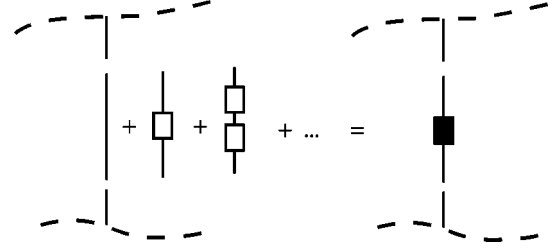
FIG. 2. Schematic dressing of particle and hole lines in the CC diagrams for matrix elements.

$$(Z_{wv})_{\text{conn}} = \sum_{\lambda=0}^{\infty} \sum_{\mu=0}^{\infty} \frac{1}{\lambda!\mu!} \langle 0_c | a_w S_w^{\dagger} (C^{\dagger})^{\lambda} \, Z \, (C)^{\mu} S_v a_v^{\dagger} | 0_c \rangle_{\text{conn}}.$$

$$(12)$$

As prescribed by the Wick theorem [12], this expression may be simplified by contracting creation and annihilation operators between various parts of this expression. Very complex structures may arise, so as a preliminary construct, consider a product $C^{\dagger}C$. Using the Wick theorem, this product may be expanded into a sum of normal forms

$$C^{\dagger}C = (C^{\dagger}C)_0 + (C^{\dagger}C)_1 + (C^{\dagger}C)_2 + \cdots$$

$$= c_0 + \sum_{ij} c_{ij}\{a_i^{\dagger}a_j\} + \frac{1}{2}\sum_{ij} c_{ijkl}\{a_i^{\dagger}a_j^{\dagger}a_l a_k\} + \cdots.$$

$$(13)$$

Here the notation $(C^{\dagger}C)_k$ stands for the k-body term. The zero-body term c_0 does not have any free particle or hole lines and would not contribute to connected diagrams of Z_{wv}. The one-body term will lead to dressing of particle and hole lines, discussed in Sec. IV. A part of the two-body term will lead to RPA-like dressing of LCCSD diagrams for matrix elements, as shown in Sec. IV.

IV. DRESSING PARTICLE AND HOLE LINES

In this section we focus on one-body term of the product $C^{\dagger}C$, Eq. (14), and derive all-order insertions for particle and hole lines. To this end it is useful to explicitly express the one-body term using particle and core labels,

$$(C^{\dagger}C)_1 = -\sum_{ab} c_{ba}a_a a_b^{\dagger} + \sum_{mn} c_{mn}a_m^{\dagger}a_n + \sum_{ma} c_{ma}a_m^{\dagger}a_a$$

$$+ \sum_{ma} c_{am}a_a^{\dagger}a_m . \qquad (14)$$

Topologically, the first term is an object where a free hole line enters some (possibly very complex) structure from above and another hole line leaves below. The second term has a similar structure but with particle lines. In Fig. 2, we draw these objects as rectangles with "stumps" indicating where the particle or hole line is to be attached. The remaining terms in Eq. (14) have both particle and hole lines involved; we will disregard these terms in the following discussion.

First we prove that given a certain CC diagram for matrix elements we may "dress" all particle and hole lines as shown

in Fig. 2. We start with a "seed" ("bare") diagram coming from a certain set of contractions in Eq. (12),

$$\frac{1}{\lambda_0!\,\mu_0!}\langle 0_c|a_w S_w^\dagger (C^\dagger)^{\lambda_0} Z (C)^{\mu_0} S_v a_v^\dagger|0_c\rangle_{\text{seed}}. \qquad (15)$$

As a next step consider a subset of terms of Eq. (12), constrained as $\lambda=\lambda_0+n$, $\mu=\mu_0+n$, $n=1, 2, 3,\ldots$. In these terms carry out contractions within a product of λ_0+n $C^\dagger$ operators and μ_0+n C operators,

$$\underbrace{C^\dagger \ldots C^\dagger}_{\lambda_0+n}\ \underbrace{C \ldots C}_{\mu_0+n}$$

Within this group there are $C_{\lambda_0+n}^n \times C_{\mu_0+n}^n$ ways to pick out n pairs of operators from the two sets, C_k^n being the binomial coefficient. Once the two strings of n operators are chosen, there are $n!$ possible ways to contract into pairs the $(C^\dagger C)_1$ object. Finally, we contract the n resulting objects into a chain (see Fig. 2); there are $n!$ possible combinations. Combining all these factors, we recover the original factor $1/(\lambda_0!\,\mu_0!)$ in front of the seed diagram (15).

We may define a dressed particle line insertion ξ_{mn} in Fig. 2 as

$$\sum_{mn} \xi_{mn} a_m^\dagger a_n = \sum_{mn} \delta_{mn} a_m^\dagger a_n + (C^\dagger C)_{p\text{-}p} + ((C^\dagger C)_{p\text{-}p}(C^\dagger C)_{p\text{-}p})_{p\text{-}p}$$

$$+ \cdots ,$$

where the subscript p-p denotes that we have to keep an insertion with a single incoming and a single outgoing particle line, e.g., $(C^\dagger C)_{p\text{-}p}=\sum_{mn} c_{mn} a_m^\dagger a_n$. Notice the absence of numerical factors in front of terms of the series; this fact follows from the preceding discussion. Explicitly,

$$\xi_{mn} = \delta_{mn} + c_{mn} + \sum_r c_{mr} c_{rn} + \cdots. \qquad (16)$$

This series may be generated by iteratively solving an implicit equation

$$\xi_{mn} = \delta_{mn} + \sum_r c_{mr}\xi_{rn}. \qquad (17)$$

The very same argument holds for dressed insertions into the hole lines.

The derivation presented above can be generalized to include simultaneous dressing of *all* particle-hole lines of a given diagram, including the inner lines of the original "bare" object $(C^\dagger C)_1$ itself. Below we illustrate our dressing scheme in the case when the cluster operator is truncated at single and double excitations.

A. Singles-doubles approximation

With the truncated cluster operator the hole line insertion reads

$$c_{ba} = \sum_m \rho_{mb}^* \rho_{ma} + \frac{1}{2}\sum_{cmn} \widetilde{\rho}_{mnbc}^* \widetilde{\rho}_{mnac} \qquad (18)$$

and the particle line insertion is
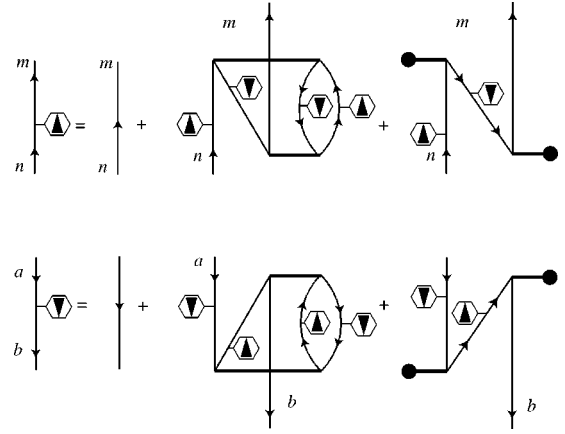
FIG. 3. Dressing of particle and hole lines in the singles-doubles approximation. The upper and lower panels represent dressing of particle and hole lines, respectively.

$$c_{mn} = -\sum_a \rho_{na}^* \rho_{ma} - \frac{1}{2}\sum_{abr} \widetilde{\rho}_{nrab}^* \widetilde{\rho}_{mrab}, \qquad (19)$$

where we introduced antisymmetric quantities $\widetilde{\rho}_{mnab}=\rho_{mnab}-\rho_{nmab}$.

Diagrammatically,

As discussed in the first part of this section, we may dress all the particle and hole lines according to the all-order scheme in Fig. 3.

Algebraically,

$$\xi_{mn} = \delta_{mn} - \sum_a \rho_{ma} R_{na}^* - \sum_{abr} \widetilde{\rho}_{mrab} R_{nrab}^*,$$

$$\xi_{ba} = \delta_{ba} - \sum_m \rho_{mb}^* R_{ma} - \sum_{mnc} \widetilde{\rho}_{mnbc}^* R_{mnac}, \qquad (20)$$

where we introduced dressed core cluster amplitudes

$$R_{na}^* = \sum_b \xi_{ba} \sum_s \rho_{sb}^* \xi_{sn},$$

$$R_{nrab}^* = \sum_t \xi_{rt} \sum_s \xi_{ns} \sum_c \xi_{ca} \sum_d \rho_{stcd}^* \xi_{db}. \qquad (21)$$

We solve Eq. (20) iteratively,

$$\xi_{mn}^{(i+1)} = \delta_{mn} - \sum_a \rho_{ma} R_{na}^{(i)*} - \sum_{abr} \widetilde{\rho}_{mrab} R_{nrab}^{(i)*},$$

$$\xi_{ba}^{(i+1)} = \delta_{ba} - \sum_m \rho_{mb}^* R_{ma}^{(i)} - \sum_{mnc} \widetilde{\rho}_{mnbc}^* R_{mnac}^{(i)}, \qquad (22)$$

where the dressed amplitudes $R_{\ldots}^{(i)}$ are to be computed with coefficients $\xi_{\ldots}^{(i)}$ obtained at the previous step.
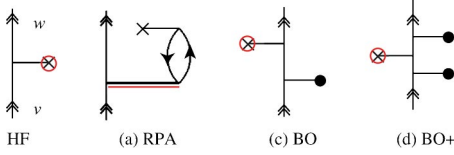
FIG. 4. Dressing of particle-hole lines in the dominant LCCSD diagrams, Fig. 1. The circled crosses represent line-dressed matrix elements, Eq. (23), and the double-lined valence cluster amplitude is the dressed amplitude, Eq. (24).

With the calculated insertions ξ we can "upgrade" the LCCSD diagrams (compare Figs. 1 and 4). To this end we introduce dressed matrix elements $\bar{z}_{ij}$ and dressed valence cluster amplitudes $R_{m\upsilon}$ and $R_{mn\upsilon a}$, similar to Eq. (21),

$$\bar{z}_{mn} = \sum_{rs} \xi_{mr} z_{rs} \xi_{sn},$$

$$\bar{z}_{ab} = \sum_{cd} \xi_{ca} z_{cd} \xi_{db}, \tag{23}$$

$$R_{m\upsilon} = \sum_{n} \xi_{mn} \rho_{n\upsilon},$$

$$R_{mn\upsilon a} = \sum_{brs} \xi_{nr} \xi_{ba} \xi_{sm} \rho_{sr\upsilon b}. \tag{24}$$

Notice that the incoming valence line in the valence amplitudes $\rho_{mn a\upsilon}$ and $\rho_{m\upsilon}$ is not dressed, since it does not represent a free end. With these objects we may dress the LCCSD diagrams, as shown in Fig. 4.

Numerically, we rigorously computed the four dressed diagrams shown in Fig. 4. In the remaining LCCSD diagrams, listed in Ref. [3], we have replaced the bare matrix elements with the dressed matrix elements, Eq. (23). Notice that the dressing of the Hartree-Fock diagram subsumes LCCSD diagrams,

$$Z_{w\upsilon}^{(g)} = -\sum_{ma} \rho_{ma}^{*} \rho_{wa} z_{m\upsilon} + \text{H.c.s.},$$

$$Z_{w\upsilon}^{(t)} = -\sum_{mnab} \rho_{mnba}^{*} \tilde{\rho}_{nwab} z_{m\upsilon} + \text{H.c.s} \tag{25}$$

from Ref. [3], so that these diagrams are to be discarded in the present approach. We postpone discussion of numerical results until Sec. VII.

V. RPA-LIKE DRESSING

In this section we continue with the systematic dressing of the coupled-cluster diagrams for matrix elements based on the topological structure of the product $C^{\dagger}C$, Eq. (14). Here we focus on the two-body term of this object. The insertion that generates the RPA-like chain of diagrams is due to a two-particle and two-hole part of the object $(C^{\dagger}C)$,
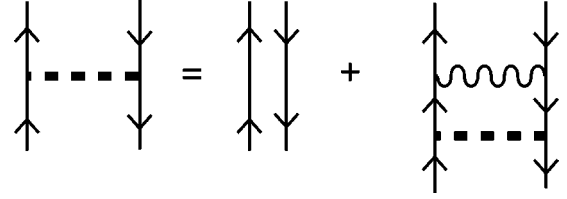
FIG. 5. Graphical equation for RPA-dressed insertion. The dashed horizontal line is the dressed insertion $\mathcal{T}_{nbma}$, while the bare object c_{nbma} is represented by a wavy line.

$$(C^{\dagger}C)_{\text{RPA}} \equiv \sum_{mnab} \tilde{c}_{nbma} \{a_{n}^{\dagger} a_{b}^{\dagger} a_{a} a_{m}\}, \tag{26}$$

where we used a symmetry property $c_{ijkl}=c_{jilk}$, and $\tilde{c}_{ijkl}=c_{ijkl}-c_{ijlk}$. An analysis identical to that presented for line dressing in Sec. IV leads us to introduce a RPA-dressed object $\mathcal{T}_{nbma}$,

$$\sum_{mnab} \tilde{\mathcal{T}}_{nbma} \{a_{n}^{\dagger} a_{b}^{\dagger} a_{a} a_{m}\} = -\sum_{mnab} \delta_{mn} \delta_{ab} \{a_{n}^{\dagger} a_{b}^{\dagger} a_{a} a_{m}\} + (C^{\dagger}C)_{\text{RPA}}$$

$$+ ((C^{\dagger}C)_{\text{RPA}}(C^{\dagger}C)_{\text{RPA}})_{\text{RPA}} + \cdots, \tag{27}$$

where the subscript RPA specifies that the objects inside the parentheses are to be contracted so that the result has the same free particle and hole ends as the original bare object $(C^{\dagger}C)_{\text{RPA}}$, Eq. (26). The sign of the leading term (with the Kronecker symbols) is chosen in such a way that a product of this term with a particle-hole object like $z_{rc}a_{c}a_{r}^{\dagger}$ results in the original object.

A detailed consideration leads to an implicit equation for the RPA-dressed particle-hole insertion

$$\tilde{\mathcal{T}}_{nbma} = -\delta_{mn}\delta_{ab} - \sum_{rc} \tilde{c}_{ncra} \tilde{\mathcal{T}}_{rbmc}. \tag{28}$$

This equation, presented graphically in Fig. 5, can be solved iteratively.

The resulting insertion $\mathcal{T}_{nbma}$ may dress any particle-hole vertex of a diagram as shown in Fig. 6.

As an example, consider dressing of particle-hole matrix elements of the operator Z: $z_{ma}a_{m}^{\dagger}a_{a}$. The equation for the dressed matrix element $\bar{z}_{ma}$ may be derived simply as

$$\bar{z}_{ma}^{\text{RPA}} \equiv -\sum_{nb} \tilde{\mathcal{T}}_{mbna} z_{nb},$$
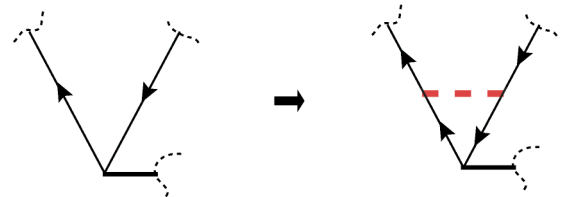
FIG. 6. Dressing particle-hole vertex of a diagram with the RPA insertion, Fig. 5.

$$\tilde{z}_{ma}^{\text{RPA}} = z_{ma} + \sum_{rc} \tilde{c}_{mcra} \sum_{nb} \tilde{\mathcal{T}}_{rbnc} z_{nb} = z_{ma} - \sum_{nb} \tilde{c}_{mbna} \tilde{z}_{nb}^{\text{RPA}},$$

where we used Eq. (28) for the dressed object $\tilde{\mathcal{T}}_{mbna}$. Finally we obtain a set of two equations

$$\tilde{z}_{am}^{\text{RPA}} = z_{am} - \sum_{nb} \tilde{c}_{mbna}^{*} \tilde{z}_{bn}^{\text{RPA}},$$

$$\tilde{z}_{ma}^{\text{RPA}} = z_{ma} - \sum_{nb} \tilde{c}_{mbna} \tilde{z}_{bn}^{\text{RPA}}.$$

The resulting equations resemble the traditional RPA formulas for dressed matrix elements (see, e.g., Ref. [15]), but do not couple $\tilde{z}_{am}^{\text{RPA}}$ and $\tilde{z}_{ma}^{\text{RPA}}$. In addition, the role of the residual Coulomb interaction of the traditional RPA formulas is played by the matrix elements of the $(C^{\dagger}C)_{\text{RPA}}$ object (which is dominated by the Coulomb interaction in the second-order; see Sec. VI). In addition, we would like to emphasize that the line-dressed matrix elements, Eq. (23), also include matrix elements between core and virtual orbitals; these are to be distinguished from the RPA-like matrix elements, Eq. (29).

The above derivation is only valid when dressing a single isolated vertex. A more complex situation arises whenever a horizontal crosscut through a diagram produces several (not just two, as in Fig. 6) unquenched particle and hole lines. Then the lower particle and hole lines of the object $(C^{\dagger}C)_{\text{RPA}}$ could be attached to the unquenched lines of the bare diagram in any order and "cross dressing" may occur. As an illustration, consider RPA dressing of the valence double contribution to the wave function $\sum_{mna} \rho_{mnva} a_m^{\dagger} a_n^{\dagger} a_a$. It arises, for example, when the diagram $Z_{wv}^{(a)}$ [see Fig. 1(a)] is cut across horizontally. The valence double contains two equivalent vertices $a_m^{\dagger} a_a$ and $a_n^{\dagger} a_a$. First we may attach the RPA object to the m-a vertex and at the second step to the n-a vertex. Apparently, this scenario is not covered by Eq. (27), since it implies that all RPA insertions are attached to the same vertex. Nevertheless, the RPA-like dressing can be carried out in a straightforward fashion. To continue with the illustration, the RPA-dressed valence double amplitude may be defined as follows [compare to Eq. (27)]

$$\sum_{mna} \mathcal{R}_{mnva}^{\text{RPA}} a_m^{\dagger} a_n^{\dagger} a_a = ([1 + (C^{\dagger}C)_{\text{RPA}}$$
$$+ ((C^{\dagger}C)_{\text{RPA}}(C^{\dagger}C)_{\text{RPA}})_{\text{RPA}} + \cdots]$$
$$\times \sum_{mna} \rho_{mnva} a_m^{\dagger} a_n^{\dagger} a_a)_{\text{val.double}}. \quad (29)$$

Here the subscript "val. double" indicates that we select a contribution having the same free ends as the right-hand side R.H.S. of the equation. The numerical factors in front of the individual RPA contributions are derived similarly to the line-dressing factors (see Sec. IV). Explicitly, we deal with a chain of diagrams

$$\mathcal{R}_{mnva}^{\text{RPA}} = \rho_{mnva} - \sum_{br} \tilde{c}_{nbra} \tilde{\rho}_{mrvb} + \sum_{bcrs} (\tilde{c}_{ncsa} \tilde{c}_{sbrc} \tilde{\rho}_{mrvb}$$
$$- \tilde{c}_{ncsa} \tilde{c}_{mbrc} \tilde{\rho}_{srvb}) + \cdots. \quad (30)$$

Examining the structure of the above expression we finally arrive at

$$\mathcal{R}_{mnva}^{\text{RPA}} = \rho_{mnva} - \sum_{sb} \tilde{c}_{nbsa} \tilde{\mathcal{R}}_{msvb}^{\text{RPA}}, \quad (31)$$

i.e., we have demonstrated how to dress the valence doubles. This example can be easily generalized to several equivalent vertices: Eq. (29) has to be rewritten using as the seed object the underlying structure of the unquenched lines produced by a horizontal crosscut through a diagram.

A. Singles-doubles approximation

Now we specialize our discussion of the RPA-like dressing to the cluster operator truncated at single and double excitations. In this CCSD approximation we obtain for the bare RPA-like insertion

$$\tilde{c}_{nbma} \approx -\rho_{mb}^{*} \rho_{na} - \sum_{rc} \tilde{\rho}_{mrbc}^{*} \tilde{\rho}_{nrac}. \quad (32)$$

Notice that one has to be careful when dealing with the first (singles × singles) term; it is represented by a disconnected diagram and may produce undesirable disconnected diagrams for matrix elements, Eq. (10).

By substituting the CCSD insertion, Eq. (32), into Eqs. (29) and (31), we immediately derive expressions for the dressed matrix elements and the RPA-dressed valence doubles. For example,

$$\mathcal{R}_{mnva}^{\text{RPA}} = \rho_{mnva} + \sum_{sb} (\sum_{rc} \tilde{\rho}_{nrac} \tilde{\rho}_{srbc}^{*}) \tilde{\mathcal{R}}_{msvb}^{\text{RPA}}, \quad (33)$$

$$\tilde{z}_{ma}^{\text{RPA}} = z_{ma} + \sum_{nb} (\sum_{rc} \tilde{\rho}_{nrbc}^{*} \tilde{\rho}_{mrac}) \tilde{z}_{nb}^{\text{RPA}}. \quad (34)$$

Here we omitted a small contribution to $\tilde{c}_{nbma}$, Eq. (32), from the product of core singles. As discussed in Sec. VI this contribution would arise in the higher orders (sixth order) of MBPT.

Practically, we notice that among the dominant LCCSD diagrams shown in Fig. 1, the particle-hole vertex occurs only in the RPA diagram $Z_{wv}^{(a)}$. Focusing on this particular diagram, the "upgraded" $Z_{wv}^{(a)}$ is simply

$$(Z_{wv}^{(a)})_{\text{dress}} = \sum_{ma} z_{am} \tilde{\mathcal{R}}_{wmva}^{\text{RPA}} + \text{H.c.s.} \quad (35)$$

Notice that the use of the RPA-dressed matrix elements to upgrade the $Z_{wv}^{(a)}$ diagram, such as

$$(Z_{wv}^{(a)})_{\text{mel.dress}} = \sum_{ma} \tilde{z}_{am}^{\text{RPA}} \tilde{\rho}_{wmva} + \text{H.c.s.}, \quad (36)$$

does not lead to the identical result, because it misses dressing of the w-a vertex. Moreover, we found numerically that dressing of both vertices, as in the more general Eq. (35), is equally important.

Finally, it is worth noting that with the RPA-like dressing scheme proposed here, the CCSD calculations would recover the entire chain of RPA diagrams. However, if the calculations of the wave functions are done using the linearized version of the coupled-cluster equations (as in Refs. [3–6]), a part of the RPA diagrams would still be missing [3]. To summarize, the inclusion of the CCSD nonlinear terms in the CC equations is crucial for a fully consistent treatment of the RPA sequence.

VI. COMPARISON WITH THE FOURTH-ORDER DIAGRAMS

The coupled-cluster method can be straightforwardly connected with the direct order-by-order many-body perturbation theory. In particular, for univalent systems, when the calculations are carried out starting from the frozen-core Hartree-Fock potential, the lowest-order contributions to the double excitation cluster amplitudes are

$$\rho_{mnva} \approx -\frac{g_{mnva}}{\varepsilon_m + \varepsilon_n - \varepsilon_a - \varepsilon_v},$$

$$\rho_{mnab} \approx -\frac{g_{mnab}}{\varepsilon_m + \varepsilon_n - \varepsilon_a - \varepsilon_b}. \quad (37)$$

Here g_{ijkl} is the matrix element of the residual (beyond the HF potential) Coulomb interaction between the electrons. It can be shown that while the LCCSD method recovers all third-order diagrams for matrix elements, it starts missing diagrams in the fourth order of MBPT. Our group has investigated these 1648 complementary fourth-order diagrams in Refs. [10,11]. Among the diagrams complementary to LCCSD matrix element contributions, there are seven terms [class $Z_{1\times2}(D_{nl})$ in Ref. [10]] due to nonlinear terms in the expansion of the CCSD wave functions; namely these $Z_{1\times2}(D_{nl})$ diagrams provide the lowest-order approximation for the dressing scheme proposed here.

In Fig. 7 we explore the topological structure of the $Z_{1\times2}(D_{nl})$ diagrams. All these diagrams come from various ways of lowest-order dressing of the $Z_{wv}^{(a)}$ diagram, Eq. (11). A comparison shows that the present dressing approach recovers five (three line-dressed and two RPA-dressed) out of seven fourth-order diagrams. The missing diagrams are shown in the bottom row of Fig. 7, and we call them "stretched" and "ladder" diagrams, the names being derived from the structure of the highlighted dressing insertions. While the ladder diagram comes from the untreated two-body contribution to the $C^\dagger C$ object, Eq. (14), the stretched diagram involves a more complex three-body contribution to $C^\dagger C$. Dressing with these two insertions can be carried out in a way similar to the line- and RPA-like dressing schemes discussed in this paper and is beyond the scope of the present analysis.

We verified that in the lowest-order MBPT approximation, Eq. (37), our dressing formulas reproduce the pertinent fourth-order expressions, explicitly presented in Ref. [10]. Furthermore, in Table I we list numerical values for individual contributions to the magnetic-dipole hyperfine-
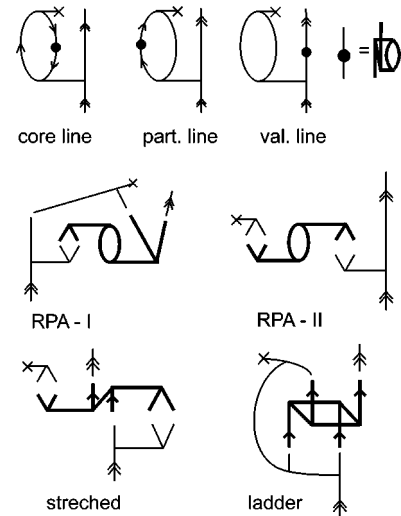
FIG. 7. Topological structure of fourth-order diagrams of class $Z_{1\times2}(D_{nl})$ derived in Ref. [10]. In these diagrams horizontal lines denote Coulomb interaction and the topological objects coming from the lowest-order approximation to $C^\dagger C$ are highlighted. The upper three diagrams arise in the leading order of the line-dressing scheme and the two diagrams in the middle are related to the RPA-dressing scheme.

structure (HFS) constant A for the ground state of ^{133}Cs and the $E1$ transition amplitude for the principal $6p_{1/2}-6s_{1/2}$ transition in Cs. Analyzing this table, we conclude that both line– and RPA–like dressing are equally important. Moreover, for these two particular matrix elements there is a partial cancellation between the line– and RPA–dressed diagrams, so that were one of the dressings omitted, the result would be misleading. We also observe that the untreated "ladder" diagram contributes a negligibly small fraction of the total. At the same time the size of the untreated "stretched" diagram indicates that (at least for the HFS constant) it is as important as the RPA-like and line-dressed diagrams.

As to the numerics, the fourth-order calculations have been carried out using relativistic B-spline basis sets as de-

TABLE I. Breakdown of contributions to $Z_{1\times2}(D_{nl})$ class of diagrams for the hyperfine-structure constant A for the $6s_{1/2}$ state and the $6s_{1/2}$-$6p_{1/2}$ electric-dipole transition amplitude for ^{133}Cs atom. The lowest-order Dirac-Hartree-Fock (DHF) values are 1425.29 MHz for the HFS constant and 5.278 a.u. for the transition amplitude. The notation $x[y]$ stands for $x \times 10^y$.

Type	$A(6s)$ (MHz)	$\langle 6s_{1/2}||D||6p_{1/2}\rangle$ (a.u.)
Core line	−2.0	7.0[−3]
Particle line	−0.90	2.5[−3]
Valence line	−0.92	0.2[−3]
RPA-I	0.005	−9.3[−3]
RPA-II	4.8	−0.05[−3]
Stretched	−3.0	0.1[−3]
Ladder	0.05	−0.008[−3]
Total	−1.9	0.41[−3]

scribed in Ref. [16]. We used a basis set of 25 out of 30 positive-energy ($\varepsilon_i > -m_e c^2$) pseudoeigenfunctions for each partial wave. Partial waves $s_{1/2}-g_{9/2}$ were included in the basis. The summation over intermediate core orbitals was limited to the eight highest-energy core orbitals for the $E1$ amplitude and included all core orbitals for the HFS constant. The reader is referred to [11] for a description of our fourth-order code.

We verified that numerical results for dressed all-order LCCSD diagrams (see Sec. VI) are consistent with the values for the pertinent fourth-order diagrams. As an example consider contributions to the $A(6s)$ HFS constant. Line dressing modifies the LCCSD $Z_{wv}^{(a)}$ diagram by -4.3 MHz in good agreement with the value of -3.8 MHz, the sum of the first three corresponding fourth-order diagrams from Table I. Similarly, RPA-like dressing modifies the $Z_{wv}^{(a)}$ diagram by $+4.4$ MHz, while the sum of fourth-order RPA diagrams from Table I is 4.8 MHz.

VII. NUMERICAL RESULTS AND DISCUSSION

To reiterate the discussion so far, we have developed the formalism of line and RPA-like dressing of the coupled-cluster diagrams for matrix elements. Further, we reduced our general formalism to the case when the cluster operator is truncated at single and double excitation amplitudes. We have also verified that in the lowest order we recover the relevant fourth-order diagrams both analytically and numerically. In this section we illustrate our all-order dressing formalism with numerical results.

We have carried out relativistic calculations of the hyperfine-structure constant A for the $6s_{1/2}$ state and $6s_{1/2}-6p_{1/2}$ electric-dipole transition amplitude for the ^{133}Cs atom. It is worth noting that matrix elements of the hyperfine interaction and the electric-dipole operator allow one to access the quality of *ab initio* wave functions both close to the nucleus and at intermediate values of the electronic coordinate. Such a test is essential for estimates of theoretical uncertainties of calculations of parity-nonconserving (PNC) amplitudes. The *ab initio* PNC amplitudes are key for high-accuracy probes of new physics beyond the standard model of elementary particles with atomic parity violation.

The results of calculations are presented in Tables II and III. In these tables we augment results of the previous all-order calculations [6] with two types of additional contributions: (i) all-order RPA and line dressing, outlined in Secs. IV and V, and (ii) complementary fourth-order contributions, so that the results are complete through the fourth-order perturbation theory. Also, for the HFS constant, we incorporate the most recent values of the Breit and radiative corrections [17,18].

LCCSD$_P$T (perturbative triples) approximation. We depart from the results of the coupled-cluster calculation described in Ref. [6]. These are linearized coupled-cluster calculations, with the wave functions truncated at single and double excitations from the reference Slater determinant. In addition, following Ref. [4], the perturbative effect of triple excitations has been incorporated into the singles-doubles equation (LCCSD$_P$T method). The main consequence of this

TABLE II. Contributions to the magnetic-dipole hyperfine-structure constant A of the ground $6s_{1/2}$ state of ^{133}Cs. LCCSD$_P$T indicates linearized coupled-cluster singles-doubles method with perturbative treatment of triples. VP + SE is the vacuum polarization and self-energy.

Contribution	Value (MHz)
DHF	1425.29
LCCSD$_P$T, Coulomb	2283.1
Breit [17]	4.6
VP+SE [18]	-9.7
LCCSD$_P$T reference	2278.0
Dressing	
Δ(line dress)	-11.0
Δ(RPA dress)	4.4
Dressing total	-6.7
Complementary fourth-order	
Triples[a]	$+17.7$
$Z_{0 \times 3}(D_{nl})$	-5.5
$Z_{1 \times 2}(D_{nl})$, stretched	-3.0
$Z_{1 \times 2}(D_{nl})$, ladder	$+0.1$
Complementary fourth-order total	$+9.3$
Final *ab initio*	2280.6
Experiment	2298.2

[a]The fourth-order contributions from triple excitations are beyond those treated in the LCCSD$_P$T approximation.

perturbative treatment is that the resulting valence removal energies are complete through the third order of perturbation energies. There is also a substantial (a few percent for Cs) improvement in the accuracy of the resulting LCCSD$_P$T hyperfine constants over the LCCSD values. At the same time the theory-experiment agreement for the $E1$ amplitudes significantly degrades (see Table III): while the LCCSD amplitudes differ by 0.4% from 0.03% accurate experimental data [22], the more sophisticated LCCSD$_P$T matrix elements deviate from measurements by as much as 1.3%. In other words, both LCCSD and LCCSD$_P$T methods are poorly suited for calculating parity-nonconserving amplitudes in ^{133}Cs with uncertainty of a few 0.1%. It is one of the goals of this paper to establish a method that will provide a consistent accuracy for both HFS constants and dipole matrix elements (and thus PNC amplitudes).

Procedure. First we solved the relativistic LCCSD$_P$T equations, as described in Ref. [6]. With the computed cluster amplitudes we calculated LCCSD$_P$T matrix elements and recovered results published in Ref. [6]. Further, we solved the line-dressing equations (22) and computed the line-dressed cluster amplitudes and matrix elements. The convergence rate was fast: four iterations were sufficient to stabilize the norms of the line-dressed cluster amplitudes at a level of a few parts per million. Finally, we solved the iterative equation for the RPA-dressed valence amplitudes, Eq. (33). It turned out to be a very computationally intensive part of the scheme and we iterated the equations only once. We used the computed RPA-dressed valence amplitudes in calculations of

TABLE III. Contributions to $\langle 6s_{1/2}||D||6p_{1/2}\rangle$ electric-dipole matrix element for Cs atom. Notation $x[y]$ stands for $x\times 10^y$.

Contribution	Value (a.u.)
DHF	5.278
LCCSD [6]	4.482
LCCSD$_P$T reference	4.558
Dressing	
Δ(line dress)	0.008
Δ(RPA dress)	−0.007
Dressing correction total	−0.001
Complementary fourth-order	
Triples[a]	−0.043
$Z_{0\times 3}(D_{nl})$	0.014
$Z_{1\times 2}(D_{nl})$, stretched	1.0[−4]
$Z_{1\times 2}(D_{nl})$, ladder	−8.6[−6]
Complementary fourth-order total	−0.029
Final *ab initio*	4.528
Experiment	
Young *et al.* [19]	4.5097(45)
Rafac *et al.* [20]	4.4890(65)
Derevianko and Porsev [21][b]	4.5064(47)
Amiot *et al.* [22][c]	4.5006(13)
Amini and Gould [23][d]	4.510(4)

[a]The fourth-order contributions from triple excitations are beyond those treated in the LCCSD$_P$T approximation.
[b]From van der Waals coefficient C_6 of the ground molecular state.
[c]Photoassociation spectroscopy; this is the most accurate determination.
[d]From static-dipole polarizability of $6s_{1/2}$ state with method of Ref. [21].

the dominant diagram $Z_{wv}^{(a)}$; see Eq. (35). In the remaining diagrams that involve particle-hole matrix elements, we employed RPA-dressed matrix elements $\bar{z}_{ij}^{\text{RPA}}$. A numerical iterative solution of equations for $\bar{z}_{ij}^{\text{RPA}}$, Eq. (34), required only a few iterations to converge to seven significant figures.

Line dressing. In Table IV we illustrate the importance of line dressing; in this table we present differences between line-dressed and bare LCCSD$_P$T diagrams for the the hyperfine constant and $E1$ amplitude. The dressing of the leading-order HF diagram subsumes the LCCSD diagrams $Z_{wv}^{(g)}$ and

TABLE IV. Line-dressing-induced modifications to dominant LCCSD$_P$T diagrams, Eq. (11), for the HFS constant A for the $6s_{1/2}$ state and the $6s_{1/2}-6p_{1/2}$ $E1$ transition amplitude for ^{133}Cs atom. Notation $x[y]$ stands for $x\times 10^y$.

Type	$A(6s)$ (MHz)	$\langle 6s_{1/2}||D||6p_{1/2}\rangle$ (a.u.)
$Z_{wv}^{(HF)}$	−22	−1.7[−3]
$Z_{wv}^{(a)}$	0.04	9.3[−3]
$Z_{wv}^{(c)}$	−8.6	−0.5[−3]
$Z_{wv}^{(d)}$	−0.8	−3.6[−5]
All diagrams	−11	8.0[−3]

$Z_{wv}^{(t)}$, Eq. (25). A direct calculation of these diagrams results in $Z_{wv}^{(g)}+Z_{wv}^{(t)}=-22.9$ MHz for $A(6s)$ and -1.75×10^{-3} a.u. for the $E1$ amplitude. These values are consistent with dressing-induced modifications of the HF diagram (-22.0 MHz and -1.7×10^{-3} a.u., respectively) from Table IV. The modifications of the $Z_{wv}^{(a)}$ diagram are consistent with the values of the pertinent fourth-order diagrams; see Sec. VI and Table I. A large dressing correction for the HFS constant comes from the diagram $Z_{wv}^{(c)}$; it is nominally a fifth-order diagram. The relative importance of this diagram is not surprising since it is based upon Brueckner orbitals (self-energy or core polarization effect). As for the $E1$ amplitude, the line-dressing correction is dominated by $Z_{wv}^{(a)}$; i.e., it is dominated by the fourth-order contribution. For the HFS constant, the relative smallness of the line-dressing correction to the $Z_{wv}^{(a)}$ diagram arises due to a delicate cancellation of relatively large contributions from dressing of the core, particle, and valence lines of the diagram (see Table I). Finally, in the bottom line of Table IV we present the difference between the line-dressed (all diagrams) and bare values. The dressing of the HF diagram plays a negligible role here, since it is dominated by the diagrams already included in the LCCSD$_P$T values. The line dressing contributes at a sizable 0.5% level to the HFS constant and at 0.2% level to the $E1$ amplitude.

RPA-like dressing. A numerically dominant contribution due to the RPA-like dressing arises for the $Z_{wv}^{(a)}$ diagram, where we used RPA-dressed valence amplitudes. The induced correction is as large as 0.2% for both dipole amplitude and HFS constant. The dressing of particle-hole matrix elements ($z_{ij}\rightarrow\bar{z}_{ij}^{\text{RPA}}$) in diagrams beyond $Z_{wv}^{(a)}$ played a relatively minor role, contributing at a level of only 0.01% for both test cases.

Complementary fourth-order diagrams. The LCCSD$_P$T method misses certain many-body diagrams for matrix elements starting from the fourth order of MBPT. These complementary corrections in the fourth order come from triple and disconnected quadruple (or nonlinear double) excitations. In Ref. [10] these corrections were classified by the role of triples and disconnected quadruples in the matrix elements (i) an *indirect* effect of triples and disconnected quadruples on single and double excitations lumped into the class $Z_{0\times 3}$; (ii) *direct* contribution to matrix elements, $Z_{1\times 2}$; (iii) corrections to normalization, Z_{norm}. A more refined classification reads

$$(Z_{wv}^{(4)})_{\text{non−LCCSD}} = Z_{1\times 2}(T_v) + Z_{1\times 2}(T_c) + Z_{0\times 3}(S_v[T_v])$$
$$+ Z_{0\times 3}(D_v[T_v]) + Z_{0\times 3}(S_c[T_c])$$
$$+ Z_{0\times 3}(D_v[T_c]) + Z_{1\times 2}(D_{nl}) + Z_{0\times 3}(D_{nl})$$
$$+ Z_{\text{norm}}(T_v) . \qquad (38)$$

Here we distinguished between valence (T_v) and core (T_c) triples and introduced a similar notation for singles (S) and doubles (D). Notation like $D_v[T_c]$ stands for the effect of core triples (T_c) on valence doubles D_v through an equation for valence doubles. The LCCSD$_P$T method combines several diagrams from $Z_{1\times 2}(T_v)$ and $Z_{0\times 3}(S_v[T_v])$ classes. We removed these already included diagrams from the fourth-

order triples in Tables II and III. The diagrams D_{nl} are contributions of disconnected quadruples. As discussed in Sec. VI one of such contributions, $Z_{1 \times 2}(D_{nl})$, provides the lowest-order approximation to our all-order dressing scheme. In Tables II and III we added the contributions of untreated "stretched" and "ladder" diagrams of the $Z_{1 \times 2}(D_{nl})$ class and also from the $Z_{0 \times 3}(D_{nl})$ class. The latter contribution would have been accounted for by solving the full (not linearized) CC equations. In our large-scale fourth-order calculations we have employed the code described in Ref. [11]; all the formulas for a large number of diagrams and the code have been generated automatically using symbolic algebra tools. While the resulting fourth-order corrections from triples are at the level of 1% , we notice that there are certain noticeable cancellations between various diagrams. Thus a complete all-order treatment of triples would be essential for attaining the next level of theoretical accuracy.

Hyperfine-constant results. Details of calculation of the hyperfine constant $A(6s_{1/2})$ are presented in Table II. To clarify the role of correlations, we first incorporate a number of small but important effects into the reference value: the Bohr-Weisskopf effect and Breit and radiative corrections. The "LCCSD$_P$T, Coulomb" value has been computed using the finite nuclear size, for both determination of wave functions and computing matrix elements of the hyperfine interaction (this accounts for 0.5% .) We also include Breit corrections from Ref. [17]; these corrections differ substantially from those incorporated in Refs. [4,6] due to order-of-magnitude important correlation corrections. Finally, radiative corrections to magnetic-dipole hyperfine-structure constants for the ground state of alkali-metal atoms were computed recently by Sapirstein and Cheng [18]. They found that the vacuum polarization and self-energy (VP+SE) contribute as much as 0.4% to the *ab initio* value. The reader should be careful with adopting Breit values from Ref. [18], because these values do not include correlation corrections (see Ref. [17] and references therein). The final value, marked as "LCCSD$_P$T reference" deviates by 0.9% from the (exact) experimental value.

Dressing corrections partially cancel, resulting in 0.3% total dressing contribution. Fourth-order diagrams, complementary to those already included in the LCCSD$_P$T value, are dominated by a contribution due to triple excitations (0.8%). We also include the "stretched" and "ladder" fourth-order diagrams missed by our dressing scheme (see Sec. VI). Almost all the correlation corrections are of similar sizes but of different signs, so the dressing and fourth-order corrections cancel, so that the final correlation correction is only 0.1%, just slightly improving the theory-experiment agreement when compared with the "LCCSD$_P$T reference" value. Our *ab initio* value for the HFS constant deviates by 0.8% from the experimental value.

Electric-dipole $6s_{1/2} - 6p_{1/2}$ transition amplitude. Details of calculation for the dipole matrix element are compiled in Table III. We do not include Breit and radiative corrections in that table, since the Breit interaction contributes only 0.02% to this matrix element [17], and radiative corrections are not known from the literature.

There were several high-accuracy experimental determinations of the $\langle 6p_{1/2} || D || 6s_{1/2} \rangle$ matrix element. We list these

matrix elements at the bottom of Table III. In Refs. [19,20] this matrix element has been extracted from the measured lifetime of the $6p_{1/2}$ state. The determination of Ref. [22] is based on photoassociative spectroscopy of cold Cs atoms (i.e., inferred from high-accuracy measurement of molecular potentials). Another approach to extraction of dipole matrix elements has been proposed by us in Ref. [21]: we exploited an enhanced sensitivity of the static electric-dipole polarizability $\alpha(0)$ of the ground state and van der Waals coefficient C_6 of the ground molecular state to the matrix elements of the principal transitions $\langle 6p_{3/2} || D || 6s_{1/2} \rangle$ and $\langle 6p_{1/2} || D || 6s_{1/2} \rangle$. Essential to the extraction of individual matrix elements was a high-accuracy ratio of these two dipole matrix elements measured in Ref. [24]. Based on the proposed method [21], the $\langle 6p_{1/2} || D || 6s_{1/2} \rangle$ matrix element has been deduced from high-accuracy C_6 in Ref. [21] and in Ref. [23] it has been inferred from $\alpha(0)$ measured in that work. The most accurate matrix element comes from photoassociation spectroscopy [22]; that result has 0.03% accuracy and we will use that value below for calibrating *ab initio* calculations.

The reference LCCSD$_P$T $E1$ matrix element deviates from high-accuracy measurements by as much as 1.3%. The correlation corrections (dressing and fourth order) computed by us improve the agreement to about 0.6%, i.e., the *ab initio* accuracy becomes comparable to that for the HFS constant. An analysis of Table III shows that due to cancellation of line- and RPA-like-dressing corrections the overall effect of dressing is negligible for this transition amplitude. At the same time, the fourth-order corrections due to triple excitations beyond LCCSD$_P$T triples are very large, almost 1% . There corrections due to residual fourth-order RPA corrections [$Z_{0 \times 3}(D_{nl})$] are also sizable, and tend to decrease the effect of triples. Our fourth-order calculation demonstrates that a full (beyond that of LCCSD$_P$T) treatment of triple excitations improves the accuracy of *ab initio* transition amplitudes.

VIII. CONCLUSION

The main two results of this work are (i) development and application of all-order dressing formalism for matrix elements computed with the coupled-cluster method; and (ii) calculations of matrix elements for Cs complete through the fourth order of many-body perturbation theory.

To reiterate, our dressing formalism is built upon a hierarchical expansion of the product of clusters $C^\dagger C$ into a sum of n-body insertions. We considered two types of insertions: particle or hole line insertion coming from the one-body part of the product and two-particle or two-hole RPA-like insertion due to the two-body part. We demonstrated how to "dress" these insertions and formulated iterative equations. Particular attention has been paid to the singles-doubles truncation of the full cluster operator and we derived the dressing equations for this popular approximation. We have upgraded coupled-cluster diagrams for matrix elements with the dressed insertions for univalent systems and highlighted the relation to pertinent fourth-order diagrams. Finally, we illus-

TABLE V. Absolute percentage deviation from high-precision data for various *ab initio* approximations.

Type	$A(6s)$	$\langle 6s_{1/2}||D||6p_{1/2}\rangle$
LCCSD	5%	0.4%
LCCSD$_P$T	0.9%	1.3%
LCCSD$_P$T+IV (this work)	0.8%	0.6%

trated our formalism with relativistic calculations for the Cs atom.

Our relativistic calculations also include a large number of fourth-order diagrams complementary to the LCCSD$_P$T method (linearized coupled-cluster single-doubles method with perturbative treatment of triples; it is the most sophisticated CC approximation applied in relativistic calculations for Cs so far). The resulting analysis is complete through the fourth order of many-body perturbation theory. We find that these complementary diagrams substantially improve the theory-experiment agreement for the important electric-dipole $6s_{1/2}$-$6p_{1/2}$ transition amplitude, and slightly improve the agreement for the hyperfine constant. To illustrate it we present in Table V the percentage deviation from high-precision data for various *ab initio* approximations. We found sizable cancellations between various fourth-order contributions; a full all-order treatment of triple and disconnected quadruple excitations is desirable to further improve the theoretical accuracy.

[1] F. Coester and H. G. Kümmel, Nucl. Phys. **17**, 477 (1960).

[2] J. Čížek, J. Chem. Phys. **45**, 4256 (1966).

[3] S. A. Blundell, W. R. Johnson, Z. W. Liu, and J. Sapirstein, Phys. Rev. A **40**, 2233 (1989).

[4] S. A. Blundell, W. R. Johnson, and J. Sapirstein, Phys. Rev. A **43**, 3407 (1991).

[5] M. S. Safronova, A. Derevianko, and W. R. Johnson, Phys. Rev. A **58**, 1016 (1998).

[6] M. S. Safronova, W. R. Johnson, and A. Derevianko, Phys. Rev. A **60**, 4476 (1999).

[7] B. K. Sahoo, G. Gopakumar, R. K. Chaudhuri, B. P. Das, H. Merlitz, U. S. Mahapatra, and D. Mukherjee, Phys. Rev. A **68**, 040501(R) (2003).

[8] G. Gopakumar, H. Merlitz, R. K. Chaudhuri, B. P. Das, U. S. Mahapatra, and D. Mukherjee, Phys. Rev. A **66**, 032505 (2002).

[9] E. Eliav, U. Kaldor, and Y. Ishikawa, Phys. Rev. A **50**, 1121 (1994).

[10] A. Derevianko and E. D. Emmons, Phys. Rev. A **66**, 012503 (2002).

[11] C. C. Cannon and A. Derevianko, Phys. Rev. A **69**, 030502(R) (2004).

[12] I. Lindgren and J. Morrison, *Atomic Many-Body Theory*, 2nd ed. (Springer-Verlag, Berlin, 1986).

[13] H. P. Kelly, Adv. Chem. Phys. **14**, 129 (1969).

[14] A. Derevianko, W. R. Johnson, and S. Fritzsche, Phys. Rev. A **57**, 2629 (1998).

[15] W. R. Johnson, Z. W. Liu, and J. Sapirstein, At. Data Nucl. Data Tables **64**, 279 (1996).

[16] W. R. Johnson, S. A. Blundell, and J. Sapirstein, Phys. Rev. A **37**, 307 (1988).

[17] A. Derevianko, Phys. Rev. A **65**, 012106 (2002).

[18] J. Sapirstein and K. T. Cheng, Phys. Rev. A **67**, 022512 (2003).

[19] L. Young, W. T. Hill III, S. J. Sibener, S. D. Price, C. E. Tanner, C. E. Wieman, and S. R. Leone, Phys. Rev. A **50**, 2174 (1994).

[20] R. J. Rafac, C. E. Tanner, A. E. Livingston, and H. G. Berry, Phys. Rev. A **60**, 3648 (1999).

[21] A. Derevianko and S. G. Porsev, Phys. Rev. A **65**, 052115 (2002).

[22] C. Amiot, O. Dulieu, R. F. Gutterres, and F. Masnou-Seeuws, Phys. Rev. A **66**, 052506 (2002).

[23] J. M. Amini and H. Gould, Phys. Rev. Lett. **91**, 153001 (2003).

[24] R. J. Rafac and C. E. Tanner, Phys. Rev. A **58**, 1087 (1998).